

Interplay of electronic correlations and chemical bonding in FeN₂ under pressure

I. V. Leonov^{1,2}

¹*M. N. Mikheev Institute of Metal Physics, Russian Academy of Sciences, 620108 Yekaterinburg, Russia*

²*Institute of Physics and Technology, Ural Federal University, 620002 Yekaterinburg, Russia*

We report a theoretical study of the effects of electronic correlations, magnetic properties, and chemical bonding in the recently synthesized high-pressure orthorhombic phase of FeN₂ using the DFT+dynamical mean-field theory approach. Our analysis documents a complex crystal-chemical behavior of FeN₂ characterized by the formation of a strongly covalent N-N bond with an unexpected valence state of Fe ions 3+ (paramagnetic ferric Fe³⁺ ions in the low-spin state), in agreement with available experimental data. Our results reveal weak (orbital-dependent) correlation effects, which are complicated by the possible emergence of multiple spin density wave states on a microscopic level. This suggests the importance of antiferromagnetic spin fluctuations to explain the properties of FeN₂ under pressure.

I. INTRODUCTION

Under high-pressure conditions crystalline solids, e.g., transition metal compounds, are known to undergo remarkable transformations associated with alterations of their quantum state and the emergence of unusual stoichiometries^{1–5}. A particular example is the binary Fe–O system. For iron oxides the high-pressure and -temperature synthesis gives numerous unexpected compositions with complex crystal structures^{6,7}. Under pressure iron oxides adopt different compositions, such as FeO₂, Fe₂O₃, Fe₃O₄, Fe₄O₅, Fe₅O₆, Fe₅O₇, Fe₇O₉, etc.,^{7–28}, with unusual crystal structures and complex electronic and magnetic properties, which can be systematized with a homologous structural series $n\text{FeO}\cdot m\text{Fe}_2\text{O}_3$ (with the exception of FeO₂)⁷.

Overall, this reflects the complexity of crystal chemistry and chemical bonding in these solids, complicated by the effects of strong electron-electron correlations in the partially occupied Fe 3*d* orbitals^{29,30}. In fact, many of these compounds exhibit a strongly correlated metallic or Mott-Hubbard (charge-transfer) insulating behavior at low pressure and temperature.

The binary transition metal-nitrogen systems and, in particular, nitrogen-rich compounds $M\text{N}_m$ with $m > 1$, are another prominent example of such complexity^{31–45}. Poly-nitrogen compounds have been considered as potential high-energy density materials, with a remarkable difference of the average bond energy between the single N–N (160 kJ mol^{–1}), double N=N (418 kJ mol^{–1}), and triple N≡N (945 kJ mol^{–1}) covalent bonds⁴⁶. Moreover, due to the strongly covalent nature of the N–N and M–N bonding these systems are often considered as candidates for ultra-hard low-compressible materials (in which short covalent bonds prevent atomic displacements resulting in exceptional mechanical properties of these solids). Nonetheless, in spite of intensive research, the crystal chemical and physical properties of the binary transition metal nitrides are still poorly understood both experimentally and theoretically to compare, e.g., with oxide materials.

Very recently the high-pressure synthesis and crystal

chemical analysis of the binary Fe–N system^{47–53} show the existence of a series different (nitrogen-rich) compositions, e.g., Fe₃N₂, FeN, FeN₂, and FeN₄, stable under pressure⁵¹. Our particular interest is devoted to the high-pressure (marcasite) phase of FeN₂, which contains both the chemical bonding of nitrogen ions (the N–N structural dimers in the lattice structure)^{46,51,52,54,55} and the effects of strong correlations and magnetic interactions (spin fluctuations) of the partially occupied Fe 3*d* states^{29,30}.

The properties of this model system (FeN₂) are also of interest in light of its structural and (partly) electronic similarity to the high-pressure pyrite phase of FeO₂ (with the $Pa\bar{3}$ crystal structure)^{23,24}. Recently synthesized under high-pressure and temperature conditions, FeO₂ has proven to be stable at the Earth's lower-mantle conditions. Because of this, FeO₂ is considered as a geologically important system with an excessive amount of oxygen. Its crystal chemical properties are exceptionally important for understanding of the Earth's lower-mantle properties, and oxygen-hydrogen cycles, have recently been widely debated in the literature^{23,24,56–64}.

It was found that FeN₂ crystallizes in the trigonal $R\bar{3}m$ structure. Upon compression above 22 GPa, FeN₂ undergoes a structural phase transition to the orthorhombic $Pnmm$ structure as documented using high-resolution powder and single-crystal synchrotron x-ray diffraction^{50,51}. The crystal structure consists of chains of edge-sharing FeN₆ octahedra aligned along the *c* axis, which are interconnected through common vertices. Both the $R\bar{3}m$ and $Pnmm$ crystal structures contain structural N–N dimers. Under pressure of about 59 GPa the nitrogen-nitrogen bond distance in FeN₂ is only 1.317 Å⁵¹, and that is intermediate between the expected bond lengths for the double N=N [N₂]^{2–} and single-bonded [N₂]^{4–} N–N bonds. For example, at ambient conditions the N=N bond length in BaN₂ is about 1.23 Å³⁹, whereas the calculated single N–N bond lengths in PtN₂ and OsN₂ (with an electronic configuration [N₂]^{4–}) are ~1.41 and 1.43 Å^{36,37}, respectively. Note that the effects of electronic correlations and chemical bonding in FeN₂ still remain unexplored. This is the main goal of our present study.

In our paper, we explore the electronic structure and magnetic properties of the high-pressure orthorhombic phase of the recently synthesized $Pnmm$ FeN_2 using the DFT+dynamical mean-field theory method to study strongly correlated materials^{65–67}. Applications of DFT+DMFT have been shown to provide a good quantitative description of the electronic structure and magnetic properties of materials with correlated electrons^{65–67}. Using DFT+DMFT it becomes possible to treat on the same footing the spin, charge, orbital, and temperature dependent interactions of the d (or f) electrons, as well as to explain a transition from localized to itinerant moment behavior near the (orbital-selective) Mott transition (under pressure, doping, or other means)^{29,30,65–67}. We discuss the effects of electron-electron correlations on the electronic structure, magnetic, and crystal chemical properties of this system.

II. METHODS

We use the DFT+DMFT method to study the spectral properties, local magnetic moments, quasiparticle mass renormalizations of the Fe $3d$ states, and magnetic correlations of the paramagnetic $Pnmm$ phase (PM) of FeN_2 under pressure (at about 59 GPa). Moreover, we perform analysis of the crystal chemical properties of FeN_2 . In our calculations, we use the lattice parameters and atomic positions obtained from the synchrotron x-ray diffraction experiments (space group $Pnmm$ with the lattice parameters $a = 4.4308$ Å, $b = 3.7218$ Å, and $c = 2.4213$ Å)⁵¹. In particular, in order to quantify the nature of chemical bonding of the N-N dimer states, e.g., the possible formation of the covalent N-N molecular orbitals, we perform analysis of the valence electron density plots and determine an electronic configuration of the Fe ion and that of the dinitrogen N-N dimer unit $[\text{N}_2]^{n-}$.

In our calculations we employ a fully charge self-consistent implementation of the DFT+DMFT method^{68–73} based on the plane-wave pseudopotential formalism within DFT¹⁹. In DFT we use generalized gradient approximation with the Perdew-Burke-Ernzerhof (PBE) exchange functional as implemented in the Quantum ESPRESSO package with ultrasoft pseudopotentials⁷⁴. In order to treat the effects of electron correlations in the partially occupied Fe $3d$ shell and charge transfer between the Fe $3d$ and N $2p$ valence states we construct a low-energy (Kohn-Sham) Hamiltonian $\hat{H}_{\sigma,mm'}^{\text{KS}}(\mathbf{k})$ using a basis set of atomic-centered Wannier functions for the Fe $3d$ and N $2p$ orbitals^{75–77}. In DFT+DMFT $\hat{H}_{\sigma,mm'}^{\text{KS}}(\mathbf{k})$ is supplemented with the on-site Coulomb term for the Fe $3d$ orbitals (in the density-density approximation):

$$\hat{H} = \sum_{\mathbf{k},\sigma} \hat{H}_{\sigma,mm'}^{\text{KS}}(\mathbf{k}) + \frac{1}{2} \sum_{\sigma\sigma',mm'} U_{mm'}^{\sigma\sigma'} \hat{n}_{m\sigma} \hat{n}_{m'\sigma'} - \hat{V}_{\text{DC}}. \quad (1)$$

Here, $\hat{n}_{m\sigma}$ is the occupation number operator (diago-

nal in the local basis set) with spin σ and orbital indices m . $U_{mm'}^{\sigma\sigma'}$ denotes the reduced density-density form of the four-index Coulomb interaction matrix: $U_{mm'}^{\sigma\sigma} = U_{mm'mm'}$ and $U_{mm'}^{\sigma\sigma'} = U_{mm'mm'} - U_{mm'm'm}$. The latter is expressed in terms of the Slater integrals F^0 , F^2 , and F^4 . For the $3d$ electrons these parameters are related to the Coulomb and Hund's coupling as $U = F^0$, $J = (F^2 + F^4)/14$, and $F^2/F^4 = 0.625$. \hat{V}_{DC} is the double-counting correction to account for the electronic interactions described within DFT. Here, we use the fully localized double-counting correction evaluated from the self-consistently determined local occupations. Our results obtained using DFT+DMFT with the around mean-field double counting (AMF) are shown in Supplemental Material (SM)⁷⁸.

We use the continuous-time hybridization expansion quantum Monte Carlo method (CT-QMC) to treat the many-body and strong correlations effects in the Fe $3d$ shell⁷⁹. In our calculations we employ the CT-QMC segment algorithm neglecting for simplicity the pair and spin-flip hopping terms of the Hund's exchange (contributions of which are typically small)⁸⁰. The effects of electron correlations in the Fe $3d$ orbitals are treated by using the on-site Hubbard $U = 6$ eV and Hund's exchange $J = 0.89$ eV, taken in accordance with previous calculations^{13,15–22}. The N $2p$ states are considered as non-correlated and are treated on the DFT level within the fully charge self-consistent DFT+DMFT approach^{17–20}. We also check different sets of the Hubbard U and Hund's exchange J values for the Fe $3d$ states. Moreover, to treat correlation effects on the partially occupied N $2p$ orbitals we perform the DFT+DMFT calculations with $U = 4$ and $J = 0.5$ eV for the N $2p$ electrons (for the Fe sites we use $U = 6$ eV and $J = 0.89$ eV). In our calculations we neglect the spin-orbit coupling effects. In order to compute the \mathbf{k} -resolved spectra we use Padé approximants to perform analytic continuation of the self-energy results on the real energy axis. In addition, we employ the maximum entropy method for analytic continuation of the Green's functions data⁸¹. Using DFT+DMFT we study the electronic structure and magnetic properties of the high-pressure PM FeN_2 at a temperature $T = 290$ K.

III. RESULTS AND DISCUSSION

A. Electronic structure

In Fig. 1 we display our results for the orbital dependent Fe $3d$ and N $2p$ spectral functions of FeN_2 calculated by DFT+DMFT at 290 K (with the crystal structure parameters taken at about 59 GPa from Ref. 51). Our results for the \mathbf{k} -resolved spectral functions are shown in Fig. 2. Our results for the spectral function agree well with those obtained by the nonmagnetic DFT (nm-DFT), suggestive of small quasiparticle mass renormalizations and, hence, weak correlations in FeN_2 under

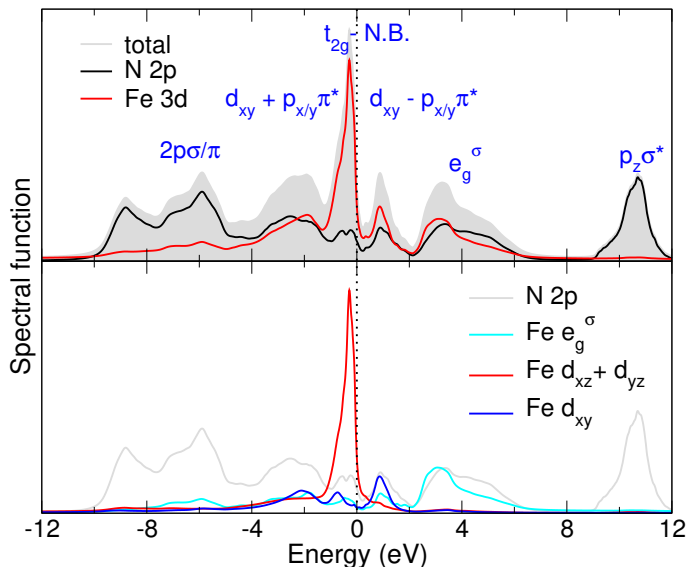


FIG. 1: Our results for the orbital-dependent spectral functions of paramagnetic FeN_2 as obtained by DFT+DMFT at $T = 290$ K. The partial Fe $3d$ ($d_{xz} + d_{yz}$, d_{xy} , and e_g^σ) and N $2p$ (bonding: $2p \sigma$ and $2p \pi$, and antibonding: $2p_{x/y} \pi^*$ and $2p_z \sigma^*$) orbital contributions are shown. Note the empty antibonding N $2p_z \sigma^*$ states located at about 10 eV above the Fermi level. While the Fe xz/yz and $x^2 - y^2/3z^2 - r^2$ orbitals are not degenerate in the orthorhombic phase of FeN_2 , the differences between them are small and for the sake of clarity only the total contributions are shown.

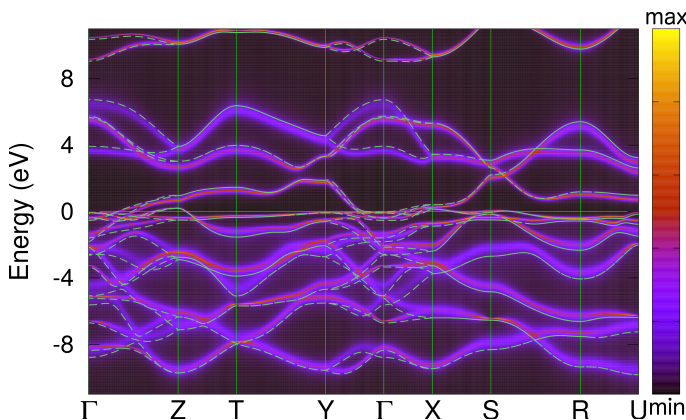


FIG. 2: \mathbf{k} -resolved spectral functions calculated by DFT+DMFT at $T = 290$ K for the orthorhombic $Pnnm$ crystal structure of FeN_2 . Our nm-DFT (PBE) results are shown with green broken green lines.

pressure (see SM⁷⁸). We obtain metal with the partially occupied Fe t_{2g} states located near the Fermi level which form coherent electronic states between -4 and 2 eV near the Fermi level. The Fe e_g^σ ($d_{x^2-y^2}$ and $d_{3z^2-r^2}$ orbitals) states are empty and appear between 2 and 6 eV above the E_F . It leads to a relatively large crystal-field splitting between the t_{2g} - e_g orbitals of about 4 eV, which in turn is suggestive of the low-spin state (LS) of Fe ions (i.e.,

crystal-field effects dominate over the Hund's exchange coupling J). In contrast to this, our DFT+DMFT results yield a relatively large (for the LS Fe^{2+} ion) instantaneous local magnetic moment value $\sqrt{\langle \hat{m}_z^2 \rangle}$ of $1.56 \mu_B$ per Fe ion, instead of the non-magnetic t_{2g} LS configuration of the Fe^{2+} ions as one can expect under high pressure. It is worth noting that the nm-DFT and DFT+DMFT calculations give a relatively large bandwidth of the N $2p$ orbitals, of about 16 eV (excluding the nonbonding N $p_z \sigma$ states located at about 10 eV above the Fermi level), implying weak correlations in the N $2p$ bands⁸².

It is also interesting to note that the crystal structure of FeN_2 determined from single-crystal x-ray diffraction experiments at about 59 GPa (space group $Pnnm$) contains the N-N structural dimers with an interatomic distance of $\sim 1.317 \text{ \AA}$ ⁵¹. This implies the possible formation of the N-N molecular bonding state in FeN_2 . In the N_2 molecule, the N-N bond length distance is about 1.1 \AA , while a charge transfer in FeN_2 yields $[\text{N}_2]^{n-}$ (with $n > 0$) with larger N-N covalent bond length (a charge transfer between Fe and N ions controls the length of the N-N bond). In agreement with this (a picture of the covalent N-N bonding) we observe a large bonding-antibonding splitting of the N $2p$ states. In fact, the bonding N $2p \sigma$ and π states are fully occupied and appear deep below the Fermi level between about -10 and -4 eV. In contrast to this the antibonding N $p_z \sigma^*$ states are empty (like in the N_2 molecule) and form bands located at about 10 eV above the E_F (see Fig. 1).

Moreover, the partially occupied π -type antibonding $[\text{N}_2]^{n-} 2p_x \pi^*$ and $2p_y \pi^*$ states appear near the Fermi level (at the place where the Fe t_{2g} states lie), strongly hybridizing with the partially occupied Fe t_{2g} states. This leads to the appearance of a complex bonding structure near the Fermi level. In particular, our results suggest the formation of a quasiparticle peak at about -0.3 eV primarily originating from the non-bonding Fe t_{2g} states (of the Fe xz and yz orbital character in the local coordinate frame with the z -axis along the shortest Fe-N bond). The non-bonding Fe xz and yz orbitals form a weakly dispersive band of about 3 eV bandwidth with a peak at about -0.3 eV below the Fermi level (it is labeled as Fe t_{2g} -N.B. in Fig. 1).

At the same time, the Fe xy and N $p_{x/y} \pi^*$ orbitals form bonding and antibonding combinations, the $d_{xy} + p_{x/y} \pi^*$ and $d_{xy} - p_{x/y} \pi^*$ molecular orbital states, respectively, which are partially occupied and are located between -4 and 2 eV near the E_F . We find that the bonding $d_{xy} + p_{x/y} \pi^*$ orbitals are fully occupied and appear at -2.1 eV below E_F , while the antibonding states are empty and are at about 0.9 eV above the Fermi level. It gives a relatively large bonding-antibonding splitting of ~ 3 eV between the $d_{xy} + p_{x/y} \pi^*$ and $d_{xy} - p_{x/y} \pi^*$ states. Overall, the Fe t_{2g} spectrum exhibits a three peak structure which is a typical characteristic feature of strongly correlated metals (with a quasiparticle peak and the lower and upper Hubbard subbands). However, in FeN_2 this behavior has different origins and is associated with com-

plex bonding of the N $2p$ and Fe $3d$ states due to the formation of bonding, antibonding, and non-bonding $p-d$ orbital states with a large bonding-antibonding splitting.

B. N-N bonding

We further quantify this point by computing the valence electron density distribution (a projection of the total charge density on the ab plane cutting the N-N bond and the Fe ions). In Fig. 3 we plot our results for the valence electron density distribution obtained by DFT+DMFT for the $Pnmm$ crystal structure of FeN_2 under pressure of about 59 GPa. We note that the N-N structural dimers clearly show the formation of a strongly covalent N-N bond with a large charge density at the N-N contact, which is about 36% of a maximal electron density value. For comparison, in the pyrite-type MgO_2 peroxide with a covalent bond $[\text{O}_2]^{2-}$ this value is $\sim 21\%$ ⁵⁹. It is interesting that this differs qualitatively from the previously obtained DFT+DMFT results for the pyrite-structured FeO_2 in which this value was significantly smaller, only about 5%, and hence the authors claim the absence of covalent oxygen-oxygen bonding in FeO_2 (with a 1.5- valence state of oxygen)⁵⁹. Our results therefore support the formation of a strong covalent N-N bond in FeN_2 under pressure, in agreement with experimental data⁵¹.

While the electronic structure of FeN_2 near the Fermi level strongly resembles that of FeO_2 , the main distinction is that the antibonding N $2p$ π^* states appear at the E_F (in FeO_2 these are the O $2p$ σ^*). Furthermore, in FeN_2 a strongly covalent N-N bonding results in a large bonding-antibonding splitting of the $2p$ states, with the N $2p_z$ σ^* states located well above E_F , at ~ 10 eV.

As we noted the calculated spectral functions of PM FeN_2 show the empty antibonding $d_{xy} - p_{x/y}\pi^*$ states located above E_F , implying that the Fe t_{2g} states are partially occupied. Our results therefore suggest that instead of a formal valence state of iron Fe^{2+} and the double-bonded N=N dimer $[\text{N}_2]^{2-}$ in FeN_2 , we deal with the ferric Fe^{3+} ions. Interestingly, this result is in accordance with the Fe^{3+} valence state previously proposed in the cubic pyrite-structured FeO_2 ^{59,61}. This result is also consistent with our estimate of the total charge at the Fe site inside the atomic sphere with a radius ~ 0.78 Å (an integral of the charge density around the Fe site with a given ionic radius) which gives 4.86 electrons, i.e., a nearly $\text{Fe}^{3+} 3d^5$ state. A similar estimate for a radius 0.9 Å gives 5.61. Note that the DFT+DMFT (AMF) calculations give 4.88 and 5.57 electrons, respectively. Overall, we found that the total charge at the Fe site is robust, varying within $\sim 1\%$ upon changing the Hubbard U and Hund's coupling J within 4-6 eV and 0.45-0.89 eV, respectively, for the Fe sites, as well as upon applying the Coulomb correlations on the N $2p$ orbitals. Moreover, the Fe^{3+} ion in the low-spin state is consistent with a relatively large (instantaneous) local moment value of about

1.56 μ_B per Fe ion. In accordance with this, our analysis of the weights of different spin-state configurations of the Fe $3d$ electrons (fluctuating between various atomic configurations within DMFT) shows a predominant low-spin configuration with a weight of 66%, with a notable admixture of the intermediate-spin states (17%).

We note that an unexpected valence state of Fe^{3+} ions implies that the N-N dimer states adopt a formal electronic configuration $[\text{N}_2]^{3-}$. Most importantly, this result agrees well with our analysis of the N-N bond lengths. In fact, the N-N bond length of about 1.317 Å in FeN_2 is found to be intermediate to those expected for the double and single-bonded N-N dimers⁵¹. In particular, at ambient conditions the N=N bond lengths in BaN_2 (the $[\text{N}_2]^{2-}$ state) is about 1.23 Å³⁹, whereas the calculated N-N bond lengths in $[\text{N}_2]^{4-}$ in PtN_2 and OsN_2 are significantly higher, about 1.41 and 1.43 Å, respectively^{36,37}. Comparing the N-N bond length in FeN_2 (1.317 Å) with previous estimates of the characteristic bond lengths, e.g., with the N-N bond lengths typical for the N_2 (~ 1.1 Å), $[\text{N}_2]^{2-}$ (1.23-1.27 Å), and $[\text{N}_2]^{3-}$ (1.30-1.34 Å) molecular orbital complexes⁵³, we propose that the N-N dimers adopt a valence state close to $[\text{N}_2]^{3-}$. While previous reports suggest the possible formation of the $[\text{N}_2]^{2-} + \bar{e}$ electrone-like state^{83,84} in the Fe-N systems^{39,41}, our analysis of the electronic structure gives no evidence for this state. In contrast to this, our results suggest strong bonding of the N $2p_{x/y}$ π^* and Fe d_{xy} states near the Fermi level, which in turn stabilizes the $[\text{N}_2]^{3-}$ radical ions.

C. Quasiparticle mass renormalizations and magnetic correlations

Next, we discuss the effects of electron correlations on the electronic structure and magnetic properties of FeN_2 under pressure. Our results for the Fe $3d$ self-energies analytically continued on the real energy axis $\Sigma(\omega)$ using Padé approximants are shown in Fig. 4. Our results for the Fe $3d$ self-energies on the Matsubara contour suggests a typical Fermi liquid-like behavior, with highly coherent spectral weights and weak quasiparticle damping of the Fe $3d$ states. Thus, $\text{Im}[\Sigma(i\omega_n)] \sim 0.03$ and 0.05 eV for the Fe t_{2g} and e_g^σ orbitals at the first Matsubara frequency, respectively, at $T = 290\text{K}$. Moreover, our DFT+DMFT calculations reveal weak renormalizations of the Fe $3d$ states $m^*/m = [1 - \partial\text{Im}[\Sigma(i\omega)]/\partial i\omega]_{i\omega \rightarrow 0}$, $\sim 1.2-1.4$, with no formation of the lower and upper Hubbard subbands in the Fe $3d$ spectral function. In addition, $\Sigma(\omega)$ gives no non-trivial poles in the \mathbf{k} -resolved Green's function (see Fig. 4) defined as $\det[\hat{H}^{\text{DFT}}(\mathbf{k}) + \text{Re}\hat{\Sigma}(\omega) - \omega] = 0$ ⁸⁵. Our analysis suggests weak (orbital-dependent) correlation effects with $m^*/m \sim 1.4, 1.3$, and 1.2 for the Fe xz/yz , xy , and e_g^σ states, respectively. We note that the quasiparticle band renormalizations depend weakly on the choice of the double counting scheme within DFT+DMFT. Using DFT+DMFT (AMF) we obtain $m^*/m \sim 1.5, 1.4$ and 1.2 for the Fe xz/yz , xy ,

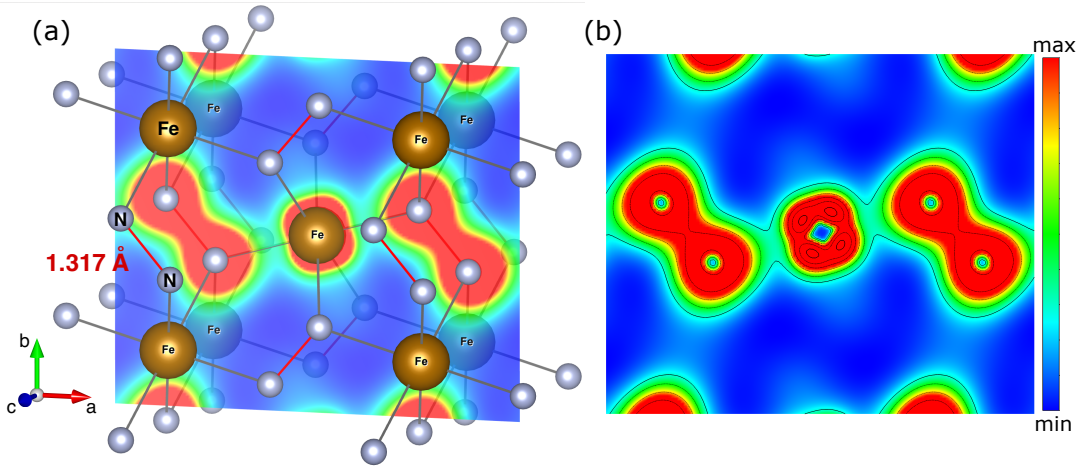


FIG. 3: Crystal structure and valence electron density plots obtained by DFT+DMFT at $T = 290$ K for the $Pnnm$ crystal structure of FeN_2 (under pressure about 59 GPa). The N-N dimer with a bond length distance ~ 1.317 Å in (a) is shown in red. Max stands for 25% of maximum of charge density $\rho(\mathbf{r})$. Our results of the DFT+DMFT (AMF) calculations are given in SM⁷⁸.

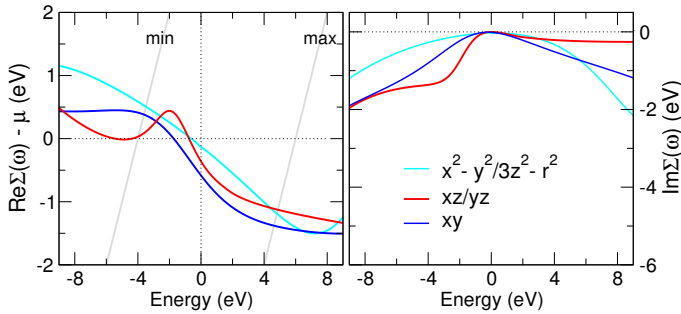


FIG. 4: Our results for the orbital-dependent Fe 3d self-energies obtained by DFT+DMFT at $T = 290$ K analytically continued on the real energy axis $\Sigma(\omega)$ using Padé approximants. min (max) stands for the minimal (maximal) energy range of the Fe 3d bands obtained within nm-DFT. Intersections with the real part of the self-energies roughly give the poles of the \mathbf{k} -resolved Green's function, as determined by $\det[\hat{H}^{\text{DFT}}(\mathbf{k}) + \text{Re}\hat{\Sigma}(\omega) - \omega] = 0$. The non-trivial solutions of this equation show the position of the lower and upper Hubbard subbands⁸⁵. Our analysis shows the absence of the Hubbard subbands in the electronic structure of FeN_2 , implying a weakly correlated (itinerant) behavior of the Fe 3d electrons.

and e_g^σ orbitals, respectively. Moreover, our results for m^*/m show a rather weak dependence upon variations of the Hubbard U and Hund's exchange J parameters. In particular, for $U = 4$ eV and $J = 0.45$ eV we obtain $m^*/m \sim 1.3, 1.2$, and 1.1 for the Fe xz/yz , xy , and e_g^σ orbitals, respectively, while for $U = 6$ eV and $J = 0.45$ eV these values are $1.4, 1.3$, and 1.2 . This implies a weakly correlated (itinerant magnetic moment) behavior of the Fe 3d states in FeN_2 under pressure. In accordance with this our analysis of the orbital-dependent local spin susceptibility $\chi(\tau)$ is evaluated within DFT+DMFT (see Fig. 5). Our calculations show a fast decay of $\chi(\tau)$ for the

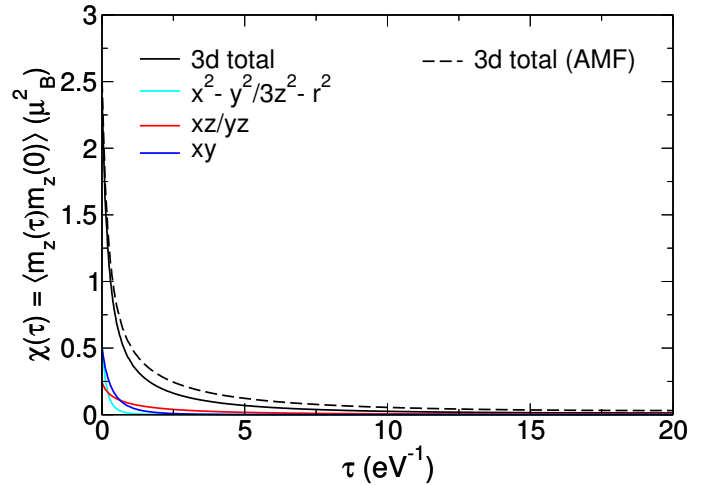


FIG. 5: Orbital-resolved local spin correlation functions $\chi(\tau) = \langle \hat{m}_z(\tau)\hat{m}_z(0) \rangle$ as a function of the imaginary time τ for the Fe 3d orbitals calculated by DFT+DMFT for FeN_2 at $T = 290$ K. Our results obtained by DFT+DMFT with the around mean-field double counting are depicted as AMF.

Fe 3d states to about $0.01 \mu_B^2$ at $\tau = \beta/2$. It is consistent with our estimate of the fluctuating moment evaluated as $M_{\text{loc}} \equiv [k_B T \int \chi(\tau) d\tau]^{1/2}$ (where $\chi(\tau) \equiv \langle \hat{m}_z(\tau)\hat{m}_z(0) \rangle$ is the local spin correlation function), of about $0.3 \mu_B$, which differs significantly from the instantaneous moments $1.56 \mu_B$ [$\langle \hat{m}_z^2 \rangle \equiv \chi(\tau = 0)$].

Finally, we study the effects of long-range magnetic correlations characterized by an ordering wave vector driven by the nesting wave vector of the Fermi surface of FeN_2 . For PM FeN_2 we determine the momentum-dependent static magnetic susceptibility $\chi(\mathbf{q})$ in the particle-hole bubble approximation within DFT+DMFT as $\chi(\mathbf{q}) = -k_B T \text{Tr} \sum_{\mathbf{k}, i\omega_n} G_{\mathbf{k}}(i\omega_n) G_{\mathbf{k}+\mathbf{q}}(i\omega_n)$, where

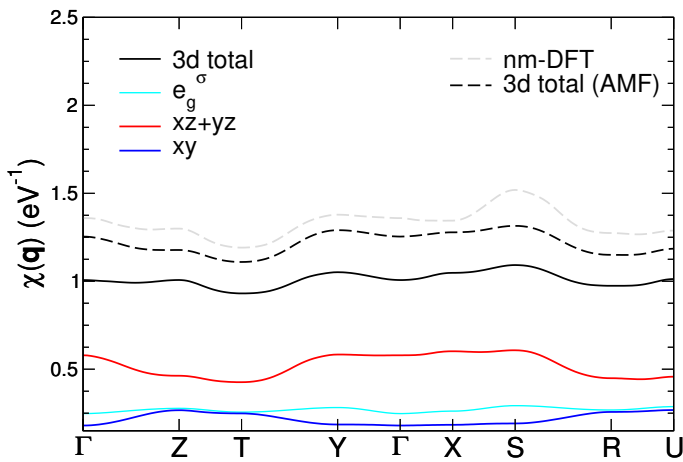


FIG. 6: Orbitally resolved static spin susceptibility $\chi(\mathbf{q})$ of Fe ions calculated by DFT+DMFT for the high-pressure orthorhombic FeN₂ at $T = 290$ K. For comparison we show the Fe 3d total $\chi(\mathbf{q})$ results obtained by the nm-DFT and DFT+DMFT (AMF) calculations. $\chi(\mathbf{q})$ is evaluated as $\chi(\mathbf{q}) = -k_B T \text{Tr} \Sigma_{\mathbf{k}, i\omega_n} G_{\mathbf{k}}(i\omega_n) G_{\mathbf{k}+\mathbf{q}}(i\omega_n)$, where $G_{\mathbf{k}}(i\omega_n)$ are the matrix elements of the local Green's function for the Fe 3d states.

$G_{\mathbf{k}}(i\omega_n)$ are the matrix elements of the local *interacting* Green's function for the Fe 3d states evaluated on the Matsubara contour $i\omega_n$. To compute $\chi(\mathbf{q})$ we take a trace over the orbital indices, denoted by Tr. Our results for $\chi(\mathbf{q})$ are shown in Fig. 6. $\chi(\mathbf{q})$ is seen to show multiple well-defined maxima, suggesting a complex interplay between different spin density wave states (with commensurate wave vectors) in FeN₂ under pressure. We note that the most pronounced instability is associated with a wave vector S ($\frac{1}{2} \frac{1}{2} 0$), competing with two minor instabilities at the X ($\frac{1}{2} 0 0$) and Y ($0 \frac{1}{2} 0$) points of the Brillouin zone. Moreover, our results for $\chi(\mathbf{q})$ remain qualitatively the same upon variations of the U and J values, with the most pronounced instability at S, competing with two minor instabilities at the X and Y points. This implies the possible emergence of long-range multiple (or intertwined) spin density wave ordering states in

FeN₂ at low pressures. This may lead to the emergence of antiferromagnetic spin fluctuations in FeN₂ which makes this system a possible candidate for spin-fluctuation mediated superconductivity. This subject deserves further detailed theoretical and experimental research.

IV. CONCLUSIONS

In conclusion, using the DFT+DMFT method we computed the electronic structure and magnetic properties of PM FeN₂ under high pressure. Our analysis of the electronic states in FeN₂ shows complex crystal-chemical behavior characterized by the formation of a strong covalent N-N bond, in agreement with experimental data⁵¹. Our results show the formations of an unexpected valence state of iron Fe³⁺ (i.e., Fe ions are ferric and low-spin paramagnetic), with the N-N dimer states adopting an electronic configuration [N₂]³⁻. This result agrees with previous estimates of the characteristic bond lengths for the [N₂]ⁿ⁻ molecular orbital complexes for different nitrogen-based systems. Our results suggest weak (orbital-dependent) correlation effects in FeN₂, which are complicated by the possible emergence of multiple (intertwined) spin density wave states on a microscopic level. This suggests the importance of antiferromagnetic ordering and spin fluctuations to explain the properties of FeN₂ under pressure. Overall, this topic deserves further detailed experimental and theoretical analysis. In this respect applications of perturbative techniques such as the GW method might be reasonable to treat the electronic correlations without a separation of the Fe 3d and N 2p orbitals into correlated and uncorrelated subspaces⁸⁶⁻⁹³. We leave this challenging problem for the future.

Acknowledgments

We acknowledge the support of the Ministry of Science and Higher Education of the Russian Federation, project No. 122021000038-7 (theme ‘‘Quantum’’).

¹ P. F. McMillan, Chemistry at high pressure. Chem. Soc. Rev. **35**, 855 (2006).
² M. Miao, Y. Sun, E. Zurek, and H. Lin, Chemistry under high pressure, Nat. Rev. Chem. **4**, 508 (2020).
³ L. Zhang, Y. Wang, J. Lv, and Y. Ma, Materials discovery at high pressures, Nat. Rev. Mater. **2**, 17005 (2017).
⁴ A. R. Oganov, C. J. Pickard, Q. Zhu, and R. J. Needs, Structure prediction drives materials discovery, Nat. Rev. Mater. **4**, 331 (2019).
⁵ L. Dubrovinsky, S. Khandarkhaeva, T. Fedotenko, D. Laniel, M. Bykov, C. Giacobbe, E. L. Bright, P. Sedmak, S. Chariton, V. Prakapenka, A. V. Ponomareva, E. A. Smirnova, M. P. Belov, F. Tasnádi, N. Shulumba, F. Trybel, I. A. Abrikosov, and N. Dubrovinskaia, Materials

synthesis at terapascal static pressures, Nature **605**, 274 (2022).

⁶ R. Bykova, Single-Crystal X-Ray Diffraction at Extreme Conditions in Mineral Physics and Material Sciences. PhD thesis, Univ. Bayreuth (2015).

⁷ E. Bykova, L. Dubrovinsky, N. Dubrovinskaia, M. Bykov, C. McCammon, S. V. Ovsyannikov, H.-P. Liermann, I. Kupenko, A. I. Chumakov, R. Ruffer, M. Hanfland, and V. Prakapenka, Structural complexity of simple Fe₂O₃ at high pressures and temperatures, Nat. Commun. **7**, 10661 (2016).

⁸ B. Lavina and Y. Meng, Unraveling the complexity of iron oxides at high pressure and temperature: Synthesis of Fe₅O₆, Sci. Adv. **1**, e1400260 (2015).

- ⁹ B. Lavina, P. Dera, E. Kim, Y. Meng, R. T. Downs, P. F. Weck, S. R. Sutton, and Y. Zhao, Charge-ordering transition in iron oxide Fe_4O_5 involving competing dimer and trimer formation, *Nature Chem.* **8**, 501 (2016).
- ¹⁰ R. Sinmyo, E. Bykova, S. V. Ovsyannikov, C. Mccammon, I. Kuppenko, L. Ismailova, and L. Dubrovinsky, Discovery of Fe_7O_9 : A new iron oxide with a complex monoclinic structure, *Sci. Rep.* **6**, 32852 (2016).
- ¹¹ S. V. Ovsyannikov, M. Bykov, E. Bykova, K. Glazyrin, R. S. Manna, A. A. Tsirlin, V. Cerantola, I. Kuppenko, A. V. Kurnosov, I. Kantor *et al.*, Pressure tuning of charge ordering in iron oxide, *Nat. Commun.* **9**, 4142 (2018).
- ¹² S. V. Ovsyannikov, M. Bykov, S. A. Medvedev, P. G. Naumov, A. Jesche, A. A. Tsirlin, E. Bykova, I. Chuvashova, A. E. Karkin, V. Dyadkin, D. Chernyshov, and L. S. Dubrovinsky, A Room-Temperature Verwey-type Transition in Iron Oxide, Fe_5O_6 , *Angew. Chem., Int. Ed.* **59**, 5632 (2020).
- ¹³ E. Greenberg, I. Leonov, S. Layek, Z. Konopkova, M. P. Pasternak, L. Dubrovinsky, R. Jeanloz, I. A. Abrikosov, and G. K. Rozenberg, Pressure-Induced Site-Selective Mott Insulator-Metal Transition in Fe_2O_3 , *Phys. Rev. X* **8**, 031059 (2018).
- ¹⁴ K. Hikosaka, R. Sinmyo, K. Hirose, T. Ishii, and Y. Ohishi, The stability of Fe_5O_6 and Fe_4O_5 at high pressure and temperature. *Am. Mineral.* **104**, 1356 (2019).
- ¹⁵ J. Kuneš, D.M. Korotin, M. A. Korotin, V. I. Anisimov, and P. Werner, Pressure-Driven Metal-Insulator Transition in Hematite from Dynamical Mean-Field Theory, *Phys. Rev. Lett.* **102**, 146402 (2009).
- ¹⁶ K. Ohta, R. E. Cohen, K. Hirose, K. Haule, K. Shimizu, and Y. Ohishi, Experimental and Theoretical Evidence for Pressure-Induced Metallization in FeO with Rocksalt-Type Structure, *Phys. Rev. Lett.* **108**, 026403 (2012).
- ¹⁷ I. Leonov, Metal-insulator transition and local-moment collapse in FeO under pressure, *Phys. Rev. B* **92**, 085142 (2015).
- ¹⁸ I. Leonov, L. Pourovskii, A. Georges, and I. A. Abrikosov, Magnetic Collapse and the Behavior of Transition Metal Oxides at High Pressure, *Phys. Rev. B* **94**, 155135 (2016).
- ¹⁹ I. Leonov, A. O. Shorikov, V. I. Anisimov, and I. A. Abrikosov, Emergence of quantum critical charge and spin-state fluctuations near the pressure-induced Mott transition in MnO, FeO, CoO, and NiO, *Phys. Rev. B* **101**, 245144 (2020).
- ²⁰ I. Leonov, G. K. Rozenberg, and I. A. Abrikosov, Charge disproportionation and site-selective local magnetic moments in the post-Perovskite-type Fe_2O_3 under ultra-high pressures, *npj Comput. Mater.* **5**, 90 (2019).
- ²¹ S. Layek, E. Greenberg, S. Chariton, M. Bykov, E. Bykova, D. M. Trots, A. V. Kurnosov, I. Chuvashova, S. V. Ovsyannikov, I. Leonov, and G. Kh. Rozenberg, Verwey-Type Charge Ordering and Site-Selective Mott Transition in Fe_4O_5 under Pressure, *J. Am. Chem. Soc.* **144**, 10259 (2022).
- ²² E. Greenberg, R. Nazarov, A. Landa, J. Ying, R. Q. Hood, B. Hen, R. Jeanloz, V. B. Prakapenka, V. V. Struzhkin, G. Kh. Rozenberg, and I. V. Leonov, Phase transitions and spin state of iron in FeO under the conditions of Earth's deep interior, *Phys. Rev. B* **107**, L241103 (2023).
- ²³ Q. Hu, D. Y. Kim, W. Yang, L. Yang, Y. Meng, L. Zhang, and H. K. Mao, FeO_2 and FeOOH under deep lower-mantle conditions and Earth's oxygen-hydrogen cycles, *Nature (London)* **534**, 241 (2016).
- ²⁴ M. Nishi, Y. Kuwayama, J. Tsuchiya, and T. Tsuchiya, The Pyrite-type high-pressure form of FeOOH , *Nature (London)* **547**, 205 (2017).
- ²⁵ J. P. Wright, J. P. Attfield, and P. G. Radaelli, Charge ordered structure of magnetite Fe_3O_4 below the Verwey transition, *Phys. Rev. B* **66**, 214422 (2002).
- ²⁶ M. S. Senn, J. P. Wright, and J. P. Attfield, Charge order and three-site distortions in the Verwey structure of magnetite, *Nature (London)* **481**, 173 (2012).
- ²⁷ G. Perversi, E. Pachoud, J. Cumby, J. M. Hudspeth, and J. P. Wright, S. A. J. Kimber, and J. P. Attfield, Co-emergence of magnetic order and structural fluctuations in magnetite, *Nat. Commun.* **10**, 2857 (2019).
- ²⁸ E. Baldini, C. A. Belvin, M. Rodriguez-Vega, I. O. Ozel, D. Legut, A. Kozłowski, A. M. Oleś, K. Parlinski, P. Piekarczyk, J. Lorenzana, G. A. Fiete, and N. Gedik, Discovery of the soft electronic modes of the trimeron order in magnetite, *Nat. Phys.* **16**, 541 (2020).
- ²⁹ N. F. Mott, *Metal-Insulator Transitions* (Taylor & Francis, London, 1990).
- ³⁰ M. Imada, A. Fujimori, and Y. Tokura, *Metal-Insulator Transitions*, *Rev. Mod. Phys.* **70**, 1039 (1998).
- ³¹ G. V. Vajenine, G. Auffermann, Y. Prots, W. Schnelle, R. K. Kremer, A. Simon, and R. Kniep, Preparation, crystal structure, and properties of barium pernitride, BaN_2 , *Inorg. Chem.* **40**, 4866 (2001).
- ³² G. Auffermann, Y. Prots, and R. Kniep, SrN and SrN_2 : diazenides by synthesis under High N_2 -pressure. *Angew. Chem. Int. Ed.* **40**, 547 (2001).
- ³³ E. Gregoryanz, C. Sanloup, M. Somayazulu, J. Badro, G. Fiquet, H.-k. Mao, and R. J. Hemley, Synthesis and characterization of a binary noble metal nitride, *Nat. Mater.* **3**, 294 (2004).
- ³⁴ A. F. Young, Ch. Sanloup, E. Gregoryanz, S. Scandolo, R. J. Hemley, and H.-k. Mao, Synthesis of novel transition metal nitrides IrN_2 and OsN_2 , *Phys. Rev. Lett.* **96**, 155501 (2006).
- ³⁵ J. C. Crowhurst, A. F. Goncharov, B. Sadigh, C. L. Evans, P. G. Morrall, J. L. Ferreira, and A. J. Nelson, Synthesis and characterization of the nitrides of platinum and iridium, *Science* **311**, 1275 (2006).
- ³⁶ J. A. Montoya, A. D. Hernandez, C. Sanloup, E. Gregoryanz, and S. Scandolo, OsN_2 : Crystal structure and electronic properties. *Appl. Phys. Lett.* **90**, 2005 (2007).
- ³⁷ Z. W. Chen, X. J. Guo, Z. Y. Liu, M. Z. Ma, Q. Jing, G. Li, X. Y. Zhang, L. X. Li, Q. Wang, Y. J. Tian, and R. P. Liu, Crystal structure and physical properties of OsN_2 and PtN_2 in the marcasite phase, *Phys. Rev. B* **75**, 054103 (2007).
- ³⁸ J. C. Crowhurst, A. F. Goncharov, B. Sadigh, J. M. Zaug, D. Aberg, Y. Meng, and V. B. Prakapenka, Synthesis and characterization of nitrides of iridium and palladium, *J. Mater. Res.* **23**, 1 (2008).
- ³⁹ M. Wessel and R. Dronskowski, Nature of N-N Bonding within High-Pressure Noble-Metal Pernitrides and the Prediction of Lanthanum Pernitride, *J. Am. Chem. Soc.* **132**, 2421 (2010).
- ⁴⁰ S. Aydin, Y. O. Ciftci, and A. Tatar, Superhard transition metal tetranitrides: XN_4 ($\text{X} = \text{Re}, \text{Os}, \text{W}$). *J. Mater. Res.* **27**, 1705 (2012).
- ⁴¹ S. B. Schneider, M. Seibald, V. L. Deringer, R. P. Stoffel, R. Frankovsky, G. M. Friederichs, H. Laqua, V. Duppel, G. Jeschke, R. Dronskowski, and W. Schnick, High-Pressure Synthesis and Characterization of $\text{Li}_2\text{Ca}_3[\text{N}_2]_3$ -

- An Uncommon Metallic Diazenide with $[\text{N}_2]^{2-}$ Ions, *J. Am. Chem. Soc.* **135**, 16668 (2013).
- ⁴² Z. Zhao, K. Bao, D. Li, D. Duan, F. Tian, X. Jin, C. Chen, X. Huang, B. Liu, and T. Cui, Nitrogen concentration driving the hardness of rhenium nitrides, *Sci. Rep.* **4**, 4797 (2014).
- ⁴³ X. Wang, J. Li, N. Xu, H. Zhu, Z. Hu, and L. Chen, Layered polymeric nitrogen in RbN_3 at high pressures, *Sci. Rep.* **5**, 16677 (2015).
- ⁴⁴ Y. Zhang, L. Wu, B. Wan, Y. Lin, Q. Hu, Y. Zhao, R. Gao, Z. Li, J. Zhang, and H. Gou, Diverse ruthenium nitrides stabilized under pressure: a theoretical prediction, *Sci. Rep.* **6**, 33506 (2016).
- ⁴⁵ M. Bykov, S. Chariton, H. Fei, T. Fedotenko, G. Aprilis, A. V. Ponomareva, F. Tasnádi, I. A. Abrikosov, B. Merle, P. Feldner, S. Vogel, W. Schnick, V. B. Prakapenka, E. Greenberg, M. Hanfland, A. Pakhomova, H.-P. Liermann, T. Katsura, N. Dubrovinskaia, and L. Dubrovinsky, High-pressure synthesis of ultraincompressible hard rhenium nitride pernitride $\text{Re}_2(\text{N}_2)(\text{N})_2$ stable at ambient conditions, *Nat. Commun.* **10**, 2994 (2019).
- ⁴⁶ Y.-R. Luo, *Comprehensive Handbook of Chemical Bond Energies*. (CRC Press, Boca Raton 2007).
- ⁴⁷ K. Suzuki, H. Morita, T. Kaneko, H. Yoshida, and H. Fujimori, Crystal structure and magnetic properties of the compound FeN , *J. Alloys. Compd.* **201**, 11 (1993).
- ⁴⁸ W. P. Clark, S. Steinberg, R. Dronskowski, C. McCammon, I. Kupenko, M. Bykov, L. Dubrovinsky, L. G. Akselrud, U. Schwarz, and R. Niewa, High-Pressure NiAs-Type Modification of FeN , *Angew. Chem. Int. Ed.* **56**, 7302 (2017).
- ⁴⁹ D. Laniel, A. Dewaele, and G. Garbarino, High Pressure and High Temperature Synthesis of the Iron Pernitride FeN_2 , *Inorg. Chem.* **57**, 6245 (2018).
- ⁵⁰ D. Laniel, A. Dewaele, S. Anzellini, and N. Guignot, Study of the iron nitride FeN into the megabar regime, *J. Alloy. Compd.* **733**, 53 (2018).
- ⁵¹ M. Bykov, E. Bykova, G. Aprilis, K. Glazyrin, E. Koemets, I. Chuvashova, I. Kupenko, C. McCammon, M. Mezouar, V. Prakapenka, H.-P. Liermann, F. Tasnádi, A. V. Ponomareva, I. A. Abrikosov, N. Dubrovinskaia, and L. Dubrovinsky, Fe-N system at high pressure reveals a compound featuring polymeric nitrogen chains, *Nat. Commun.* **9**, 2756 (2018).
- ⁵² M. Bykov, S. Khandarkhaeva, T. Fedotenko, P. Sedmak, N. Dubrovinskaia, and L. Dubrovinskya, Synthesis of FeN_4 at 180 GPa and its crystal structure from a submicron-sized grain, *Acta Crystallogr. E: Crystallogr.* **74**, 1392 (2018).
- ⁵³ D. Laniel, B. Winkler, T. Fedotenko, A. Aslandukova, A. Aslandukov, S. Vogel, T. Meier, M. Bykov, S. Chariton, K. Glazyrin, V. Milman, V. Prakapenka, W. Schnick, L. Dubrovinsky, and N. Dubrovinskaia, High-pressure $\text{Na}_3(\text{N}_2)_4$, $\text{Ca}_3(\text{N}_2)_4$, $\text{Sr}_3(\text{N}_2)_4$, and $\text{Ba}(\text{N}_2)_3$ featuring nitrogen dimers with noninteger charges and anion-driven metallicity, *Phys. Rev. Mater.* **6**, 023402 (2022).
- ⁵⁴ M. Wessel and R. Dronskowski, A New Phase in the Binary Iron Nitrogen System?—The Prediction of Iron Pernitride, FeN_2 . *Chem. Eur. J.* **17**, 2598 (2011).
- ⁵⁵ Z. Wang, Y. Li, H. Li, I. Harran, M. Jia, H. Wang, Y. Chen, H. Wang, and N. Wu, Prediction and characterization of the marcasite phase of iron pernitride under high pressure, *J. Alloy. Compd.* **702**, 132 (2017).
- ⁵⁶ E. Boulard, M. Harmand, F. Guyot, G. Lelong, G. Morard, D. Cabaret, S. Boccato, A. D. Rosa, R. Briggs, S. Pascarelli, and G. Fiquet, Ferrous iron under oxygen-rich conditions in the deep mantle, *Geophys. Res. Lett.* **46**, 1348 (2019).
- ⁵⁷ J. Liu, Q. Hu, W. Bi, L. Yang, Y. Xiao, P. Chow, Y. Meng, V. B. Prakapenka, H. K. Mao, and W. L. Mao, Altered chemistry of oxygen and iron under deep earth conditions, *Nat. Commun.* **10**, 153 (2019).
- ⁵⁸ Q. Hu and J. Liu, Deep mantle hydrogen in the pyrite-type $\text{FeO}_2\text{-FeO}_2\text{H}$ system, *Geosci. Front.* **12**, 975 (2020).
- ⁵⁹ E. Koemets, I. Leonov, M. Bykov, E. Bykova, S. Chariton, G. Aprilis, T. Fedotenko, S. Clément, J. Rouquette, J. Haines *et al.*, Revealing the Complex Nature of Bonding in the Binary High-Pressure Compound FeO_2 , *Phys. Rev. Lett.* **126**, 106001 (2021).
- ⁶⁰ B. G. Jang, D. Y. Kim, and J. H. Shim, Metal-insulator transition and the role of electron correlation in FeO_2 , *Phys. Rev. B* **95**, 075144 (2017).
- ⁶¹ S. S. Streltsov, A. O. Shorikov, S. L. Skorniyakov, A. I. Poteryaev, and D. I. Khomskii, Unexpected 3+ valence of iron in FeO_2 , a geologically important material lying in between oxides and peroxides, *Sci. Rep.* **7**, 13005 (2017).
- ⁶² A. O. Shorikov, A. I. Poteryaev, V. I. Anisimov, and S. V. Streltsov, Hydrogenation-driven formation of local magnetic moments in FeO_2H_x , *Phys. Rev. B* **98**, 165145 (2018).
- ⁶³ C. Lu, M. Amsler, and C. Chen, Unraveling the structure and bonding evolution of the newly discovered iron oxide FeO_2 , *Phys. Rev. B* **98**, 054102 (2018).
- ⁶⁴ B. G. Jang, J. Liu, Q. Hu, K. Haule, H. K. Mao, W. L. Mao, D. Y. Kim, and J. H. Shim, Electronic spin transition in FeO_2 : Evidence for Fe(II) with peroxide O_2^{2-} , *Phys. Rev. B* **100**, 014418 (2019).
- ⁶⁵ G. Kotliar and D. Vollhardt, Strongly Correlated Materials: Insights From Dynamical Mean-Field Theory, *Phys. Today* **57**, 53 (2004).
- ⁶⁶ A. Georges, G. Kotliar, W. Krauth, and M. J. Rozenberg, Dynamical Mean-Field Theory of Strongly Correlated Fermion Systems and the Limit of Infinite Dimensions, *Rev. Mod. Phys.* **68**, 13 (1996).
- ⁶⁷ G. Kotliar, S. Y. Savrasov, K. Haule, V. S. Oudovenko, O. Parcollet, and C. A. Marianetti, Electronic structure calculations with dynamical mean-field theory, *Rev. Mod. Phys.* **78**, 865 (2006).
- ⁶⁸ L. V. Pourovskii, B. Amadon, S. Biermann, and A. Georges, Self-Consistency over the Charge Density in Dynamical Mean-field Theory: A Linear Muffin-Tin Implementation and Some Physical Implications, *Phys. Rev. B* **76**, 235101 (2007).
- ⁶⁹ K. Haule, Quantum Monte Carlo impurity solver for cluster dynamical mean-field theory and electronic structure calculations with adjustable cluster base, *Phys. Rev. B* **75**, 155113 (2007).
- ⁷⁰ M. Aichhorn, L. V. Pourovskii, V. Vildosola, M. Ferrero, O. Parcollet, T. Miyake, A. Georges, and S. Biermann, Dynamical mean-field theory within an augmented plane-wave framework: Assessing electronic correlations in the iron pnictide LaFeAsO , *Phys. Rev. B* **80**, 085101 (2009).
- ⁷¹ B. Amadon, A self-consistent DFT+DMFT scheme in the projector augmented wave method: Applications to cerium, Ce_2O_3 and Pu_2O_3 with the Hubbard I solver and comparison to DFT+U, *J. Phys.: Condens. Matter* **24**, 075604 (2012).
- ⁷² H. Park, A. J. Millis, and C. A. Marianetti, Computing total energies in complex materials using charge self-

- consistent DFT+DMFT, Phys. Rev. B **90**, 235103 (2014).
- ⁷³ A. Hampel, S. Beck, and C. Ederer, Effect of charge self-consistency in DFT+DMFT calculations for complex transition metal oxides, Phys. Rev. Res. **2**, 033088 (2020).
- ⁷⁴ P. Giannozzi, S. Baroni, N. Bonini, M. Calandra, R. Car, C. Cavazzoni, D. Ceresoli, G. L. Chiarotti, M. Cococcioni, I. Dabo *et al.*, QUANTUM ESPRESSO: A Modular and Open-Source Software Project for Quantum Simulations of Materials, J. Phys. Condens. Matter **21**, 395502 (2009).
- ⁷⁵ V. I. Anisimov, D. E. Kondakov, A. V. Kozhevnikov, I. A. Nekrasov, Z. V. Pchelkina, J. W. Allen, S.-K. Mo, H.-D. Kim, P. Metcalf, S. Suga *et al.*, Full Orbital Calculation Scheme for Materials with Strongly Correlated Electrons, Phys. Rev. B **71**, 125119 (2005).
- ⁷⁶ G. Trimarchi, I. Leonov, N. Binggeli, Dm. Korotin, and V. I. Anisimov, LDA+DMFT Implemented with the Pseudopotential Plane-Wave Approach, J. Phys. Condens. Matter **20**, 135227 (2008).
- ⁷⁷ Dm. Korotin, A. V. Kozhevnikov, S. L. Skornyakov, I. Leonov, N. Binggeli, V. I. Anisimov, G. Trimarchi, Construction and solution of a Wannier-functions based Hamiltonian in the pseudopotential plane-wave framework for strongly correlated materials, Eur. Phys. J. B **65**, 91 (2008).
- ⁷⁸ See Supplemental Material at <http://link.aps.org/supplemental/> for additional figures with our DFT+DMFT results for FeN₂.
- ⁷⁹ E. Gull, A. J. Millis, A. I. Lichtenstein, A. N. Rubtsov, M. Troyer, and P. Werner, Continuous-time Monte Carlo methods for quantum impurity models, Rev. Mod. Phys. **83**, 349 (2011).
- ⁸⁰ Here, the effects of the Hund's exchange interaction J are taken into account on the density-density level, i.e., the multiplet structure of the d states is described approximately. It is critical to use the fully rotationally invariant scheme for the systems in which multiplet effects are essential, e.g., those with substantial spin-orbit coupling effects. Moreover, it is typically that the inclusion of the pair and spin-flip hopping terms of the Hund's exchange leads to additional screening of the density-density part of the Coulomb interactions and, hence, to a less correlated behavior.
- ⁸¹ A. W. Sandvik, Stochastic method for analytic continuation of quantum Monte Carlo data, Phys. Rev. B **57**, 10287 (1998).
- ⁸² In fact, our DFT+DMFT calculations for FeN₂ with the N $2p$ orbitals treated as correlated with the Hubbard $U = 4$ eV and Hund's exchange $J = 0.5$ eV (and with $U = 6$ eV and $J = 0.89$ eV for the Fe $3d$ shell) give quantitatively similar results as those with the N $2p$ states treated on the nm-DFT ($U = J = 0$ eV) level. In particular, for quasiparticle mass renormalizations we obtain $m^*/m \sim 1.4, 1.3,$ and 1.2 for the Fe $xz/yz, xy,$ and e_g^σ orbitals, respectively. It was found that quasiparticle mass renormalizations for the N $2p$ states are roughly ~ 1.1 . Our estimate of the Fe valence state (the total charge at Fe site inside the atomic sphere with a radius ~ 0.78 Å) is 4.9, corresponding to a nearly Fe $3+$ state.
- ⁸³ J. L. Dye, Electrides: Early Examples of Quantum Confinement, Acc. Chem. Res. **42**, 1564 (2009).
- ⁸⁴ C. Liu, S. A. Nikolaev, W. Ren, and L. A. Burton, Electrides: A review, J. Mater. Chem. C **8**, 10551 (2020).
- ⁸⁵ A. I. Poteryaev, J. M. Tomczak, S. Biermann, A. Georges, A. I. Lichtenstein, A. N. Rubtsov, T. Saha-Dasgupta, and O. K. Andersen, Enhanced crystal-field splitting and orbital-selective coherence induced by strong correlations in V₂O₃, Phys. Rev. B **76**, 085127 (2007).
- ⁸⁶ L. Hedin, New method for calculating the one-particle Green's function with application to the electron-gas problem, Phys. Rev. **139**, A796 (1965).
- ⁸⁷ M. Rohlfing and S. G. Louie, Electron-hole excitations and optical spectra from first principles, Phys. Rev. B **62**, 4927 (2000).
- ⁸⁸ F. Aryasetiawan and O. Gunnarsson, The GW method, Rep. Prog. Phys. **61**, 237 (1998).
- ⁸⁹ G. Onida, L. Reining, and A. Rubio, Electronic excitations: density-functional versus many-body Green's-function approaches, Rev. Mod. Phys. **74**, 601 (2002).
- ⁹⁰ P. Sun and G. Kotliar, Extended dynamical mean-field theory and GW method, Phys. Rev. B **66**, 085120 (2002).
- ⁹¹ M. van Schilfhaarde, T. Kotani, and S. Faleev, Quasiparticle Self-Consistent GW Theory, Phys. Rev. Lett. **96**, 226402 (2006).
- ⁹² J. Klimeš, M. Kaltak, and G. Kresse, Predictive GW calculations using plane waves and pseudopotentials, Phys. Rev. B **90**, 075125 (2014).
- ⁹³ T. Zhu and G. K.-L. Chan, Ab Initio Full Cell GW+DMFT for Correlated Materials, Phys. Rev. X **11**, 021006 (2021).